Chapter 5
Photocontrol of Antibacterial Activity: Shifting from UV to Red Light Activation

The field of photopharmacology aims to introduce smart drugs that, through the incorporation of molecular photoswitches, allow for the remote spatial and temporal control of bioactivity by light. This concept could be particularly beneficial in the treatment of bacterial infections, by reducing the systemic and environmental side-effects of antibiotics. A major concern in the realization of such light-responsive drugs is the wavelength of the light that is applied. Studies on the photocontrol of biologically active agents mostly rely on UV light, which is cytotoxic and poorly suited for tissue penetration. In our efforts to develop photoswitchable antibiotics, we introduce here antibacterial agents whose activity can be controlled by visible light, while getting into the therapeutic window. For that purpose, a UV light-responsive core structure based on diaminopyrimidines with suitable antibacterial properties was identified. Subsequent modification of an azobenzene photoswitch moiety lead to structures that allowed us to control their activity against Escherichia coli in both directions with light in the visible region. For the first time, full in situ photocontrol of antibacterial activity in the presence of bacteria was attained with green and violet light. Most remarkably, one of the diaminopyrimidines revealed an at least eight-fold difference in activity before and after irradiation with red light at 652 nm, showcasing the effective "activation" of a biological agent otherwise inactive within the investigated concentration range, and doing so with red light in the therapeutic window.

This chapter was published as: **Photocontrol of Antibacterial Activity: Shifting from UV to Red Light Activation.** M. Wegener,* M. J. Hansen,* A. J. M. Driessen, W. Szymanski, B. L. Feringa, *J. Am. Chem. Soc.* **2017**, *139*, 17979–17986 (* equal contribution).

5.1 Introduction

The often life-saving treatment of infectious diseases is increasingly compromised by the emergence of antimicrobial resistance,[1–4] which can be traced back to a build-up of antibiotics in the environment due to their excessive application in both human health care and animal husbandry.[5–7] Another issue that plagues especially long-term antibiotic treatment is the common occurrence of severe adverse effects. A highly relevant case can be found in the fluoroquinolone antibiotics.[8,9] Quinolones are a class of synthetic, broad-spectrum antibiotics widely relied upon in the clinic since their discovery in the 1960s;[4] however, safety concerns regarding the treatment with fluoroquinolones are still being raised, with the FDA issuing the latest of numerous warnings as recently as 2016[10] (risks include selection of resistant pathogens,[11] tendon rupture[12] and nerve damage[13]). Such a decline in the reliability of long-established classes of antibiotics is particularly troubling in the face of resistant pathogenic bacteria and the slow pace of innovation in antibacterial drug discovery over the last five decades.[14,15]

The emerging fields of photopharmacology[16–19] and photochemotherapy[20–28] offer a promising approach to deal with both systemic and environmental side-effects resulting from chemotherapy (Figure 1). Rendering a drug photoswitchable allows for the spatial and temporal control over its biological activity with light. Light is, in principle, not harmful and easily delivered with high precision, which has already lead to its application in antibacterial photodynamic therapy[29–32] for the formation of singlet oxygen. Examples of the successful utilization of photopharmacology, which is singlet oxygen independent, include photoswitchable antimicrobials[33–36] and anti-tumor therapy,[37–39] control of neuronal networks,[40,41] and vision restoration.[42,43] However, so far, the application of photopharmacology in a reversible manner (on/off switching of bioactivity with light) is often limited by the need of UV light to effect photoisomerization. UV light is toxic to healthy cells[44] and has a limited tissue penetration depth.[45,46] To ultimately realize their full potential by achieving reversible control of activity *in vivo* (Figure 1c), photopharmacological agents should ideally be responsive to light in the therapeutic window between 650 and 900 nm.[45,46]

In our effort to create photoswitchable antimicrobials while addressing the challenge to use visible or red light, we focused on antifolates, particularly in the antibiotic trimethoprim as a starting point for structural design. Antifolates are a class of drugs that interfere with the biosynthesis of folate, by inhibition of dihydrofolate reductase (DHFR) which catalyzes the reduction of dihydrofolate to the active cofactor tetrahydrofolate.[47,48] The latter plays a vital role in the biosynthesis of essential bacterial metabolites, such as the amino acids glycine and methionine, as well as purines and thymidine triphosphate. As a result, tetrahydrofolate depletion sets off a complex cascade that ultimately leads to the cessation of DNA, RNA and protein synthesis.[49–51]

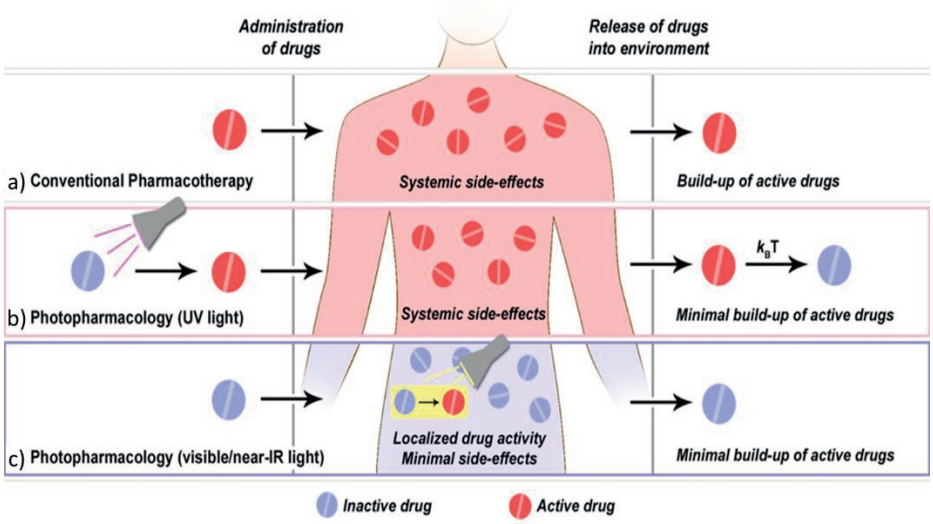

Figure 1. Potential scenarios for the application of photopharmacology compared to conventional pharmacotherapy. a) Classic chemotherapeutic treatment without control over drug activity leads to systemic side-effects and environmental build-up that is particularly damaging in the case of antibiotics, as this constitutes a major cause for the emergence of antimicrobial resistance. b) Photopharmacological agents responsive to UV light may offer only a partial solution to these issues, as a drug with suitable properties may possibly be activated before administration by UV light irradiation, with the potentially unstable active state losing its activity over time, thus counteracting the environmental build-up. c) Full control of photopharmacological agents outside as well as inside the human body to address both systemic and environmental side-effects can only be realized if the photoswitchable drug is responsive to visible or near-IR light, both not harmful to cells and, particularly in the near-IR range, better suited to penetrate tissue. In this chapter, we report, for the first time, the control of antibiotic activity with red light and show *in situ* photocontrol of antibacterial activity in the presence of bacteria.

Antifolates include antibacterial,[47,48,52] antiprotozoal[53,54] and anticancer agents.[55–57] Among these, the antibiotic trimethoprim[58–61] shows a high selectivity towards bacterial DHFR compared to mammalian DHFR.[62] It is active against a broad spectrum of Gram-positive and Gram-negative bacteria (including *Staphylococcus aureus*, *Streptococcus pneumoniae*, *Klebsiella pneumoniae*, *Escherichia coli* and *Hemophilus influenzae*) and widely used in the clinic (especially against urinary and respiratory tract infections).[63] However, treatment with trimethoprim is plagued by the emergence of bacterial resistance.[64,65] This makes it a particularly interesting candidate for photo-pharmacology, i.e. the development of photoresponsive analogues, as the spatial and temporal control over their activity could reduce excessive and unwanted exposure of bacteria to the active form of the drug, and thus drastically limit the number of bacteria with engaged resistance mechanisms.

5.2 Results and Discussion

The potential to modify the structure of trimethoprim[52,66,67] without losing affinity towards bacterial DHFR further encouraged us to use it as a basis for photoswitchable antibiotics. Initially we sought to employ a simple, modular approach to attach regular, UV light-responsive azobenzene photoswitches to the trimethoprim core structure in different ways, thus providing quick, synthetically facile access to a small collection of compounds that exhibit high structural diversity. In this way, we expected to identify a promising structural platform with the desired photopharmacological properties. Subsequent exchange of the azobenzene switch with a red-shifted analogue would enable photoisomerization with visible light, ideally with retention of the antibacterial properties.

The first stage of this approach is illustrated in Scheme 1: Photoresponsive diaminopyrimidines of the general structure **2** were generated by attachment of largely unsubstituted azobenzenes to the core structure of trimethoprim (**1**). Switches were either directly connected to the 2, 3 and 4 positions of the drug's methoxyphenyl unit by Suzuki cross-coupling (**2a-f**), or by alkylation of the free hydroxy group in the 4 position via different linkers (**2g-j**). Before starting with biological experiments, basic photochemistry of compounds **2a-j** was studied in DMSO to ensure satisfactory photoswitching behavior. In case of **2h**, NMR analysis revealed degradation of the compound upon irradiation with UV light, which was remedied by introduction of a methoxy group in 4'-position, resulting in compound **2i**.

Scheme 1. Structurally diverse set of UV light-responsive diaminopyrimidines.

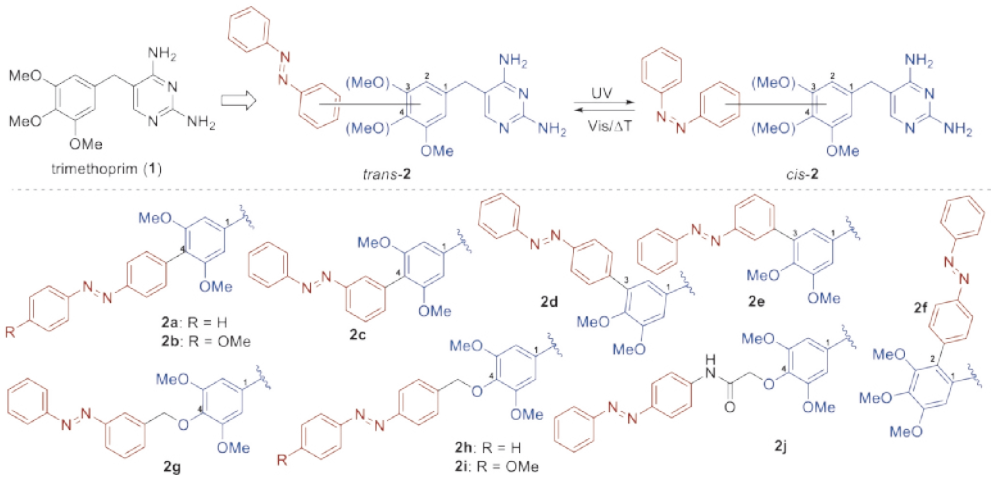

With this small library of structurally diverse compounds **2** in hand, subsequently their antibacterial activity was investigated against *E. coli* in two-fold dilution series,

both before and after irradiation with UV light at 365 nm. With the exception of **2f** and **2j**, which proved to be mostly inactive up to a concentration of 20 µM, all compounds effectively inhibited bacterial growth with various degrees of potency. When comparing inhibition of growth by irradiated and non-irradiated samples, in most cases no significant difference was observed. However, **2i** stood out in that respect, as a considerable change in potency was evident upon *trans-cis* isomerization (see growth curves in Figure 2, which translate into a MIC50 of 20 µM before and 10 µM after irradiation). Fortunately, the *cis* isomer was found to be the more active one, setting the stage for targeted structural modifications of the photoswitch to specifically red-shift the wavelength for *trans-cis* isomerization (*vide infra*). In addition, the fact that the active *cis* isomer usually has a limited half-life and thermally isomerizes to the more stable – but less active – *trans* isomer, enables an intrinsic autodeactivation pathway that would help prevent the build-up of active drugs in the environment (cf. Figure 1b).[33]

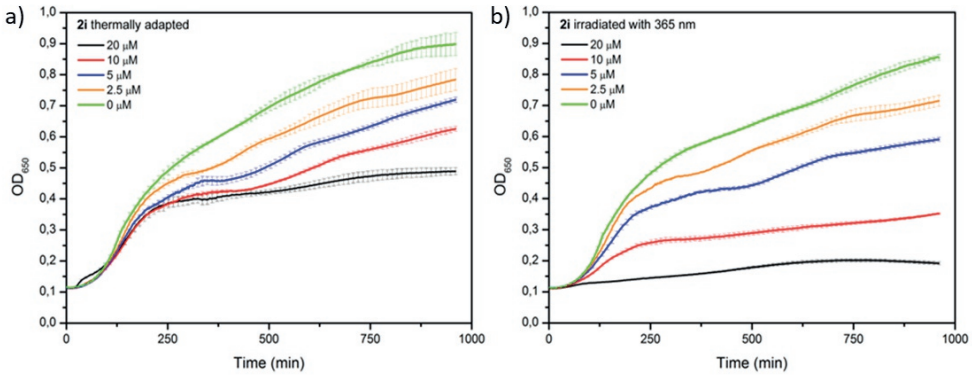

Figure 2. Bacterial growth curves of *E. coli* CS1562 at increasing concentrations of **2i**. a) Samples after thermal adaptation. b) Samples after irradiation with UV light at λ = 365 nm. Error bars show s.d. calculated from measurements in triplicate.

Prior to structural modification of **2i** to achieve the desired red-shift of its activating wavelength, we further investigated the actual nature of its observed effect on bacterial growth upon photoisomerization. From chemical actinometry and quantum yield determination, we obtained ϕ(*trans-cis*) = 0.18 and ϕ(*cis-trans*) = 0.02 for **2i** (see Figure 10), which showed that switching efficiencies are preserved when the azobenzene core was substituted with the trimethoprim motif. UV-Vis analysis of **2i** in aqueous medium at 30 µM showed some form of aggregation of the compound in its *trans* state. Upon irradiation with 365 nm (for specifications see Figure 8), the aggregates appear to dissolve during *trans-cis* isomerization, providing a possible explanation for the difference in potency. However, this effect was no longer observed at a concentration of 5 µM, whereas a difference in antibacterial activity was still evident at that concentration. Furthermore, other diaminopyrimidines **2** exhibited similar aggregation behavior upon

photoisomerization in aqueous medium, without any significant difference in activity between the respective photoisomers observed during antibacterial experiments. This encouraged us to proceed under the premise that the difference in antibacterial activity of **2i** effected by photoisomerization does indeed directly originate from structural changes on a molecular level, and is not caused by differences in solubility in the bacterial growth medium. We envisioned that further modification of the basic structure of **2i** would not only bring forth the desired red-shift of the activating wavelength, but will also resolve any issue of possible aggregation in aqueous medium.

Scheme 2. Synthesis of red-shifted diaminopyrimidines **12** and **13**.

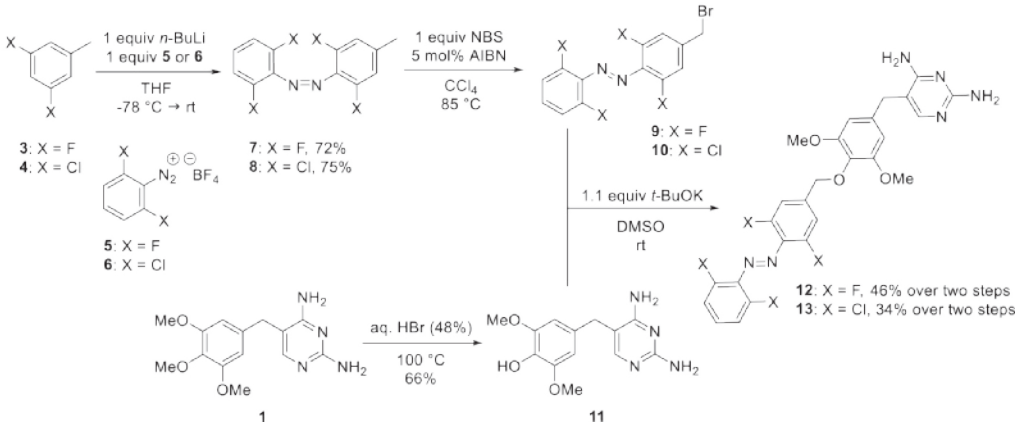

Among ongoing efforts to realize azobenzene photoswitches that can be addressed with visible light,[68–72] the groups of Hecht[73] and Woolley[74] made significant progress with the design and synthesis of azobenzenes bearing fluoro-, chloro- or methoxy-substituents in all positions ortho to the azo moiety. The influence of these substituents allows for the effective use of lower-energy n-π* excitation to trigger *trans-cis* photoisomerization. Taking advantage of this approach in the creation of red-shifted analogues of structure **2i**, we were particularly interested in the *tetra*-fluoro-substituted azobenzenes, since such a modification would provide us with a structure closest to **2i** in terms of size. In order to synthetically access the modified structure **12** (Scheme 2), we utilized the methodology, introduced in chapter 4, for the facile preparation of ortho-substituted azobenzenes:[75] Lithiation of 3,5 difluorotoluene (**3**) and subsequent conversion with the corresponding diazonium salt **5** gave azobenzene **7** in good yield. After radical bromination, bromide **9** was used in an alkylation of phenol **11**, which in turn could be directly obtained from trimethoprim (**1**) by selective ether cleavage.[67] Thus, photoresponsive diaminopyrimidine **12** was readily prepared by direct modification of the commercially available drug.

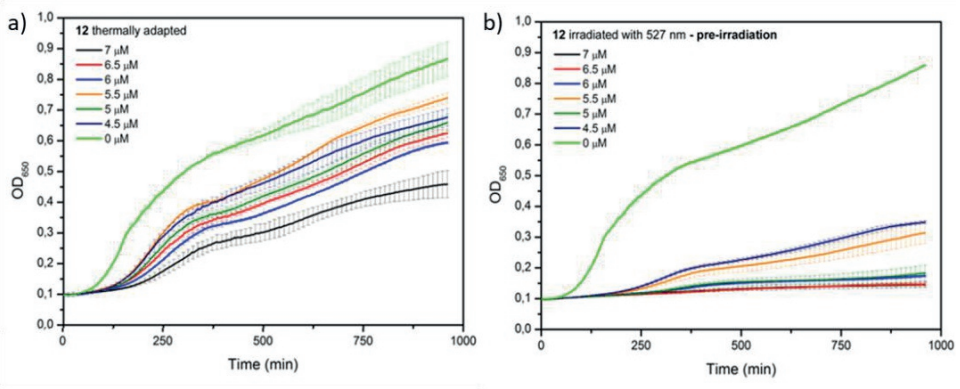

Figure 3. Bacterial growth curves of *E. coli* CS1562 at increasing concentrations of **12**. a) Samples after thermal adaptation. b) Samples after irradiation with green light at λ = 527 nm. Error bars show s.d. calculated from measurements in triplicate.

Efficient *trans-cis* isomerization of **12** in DMSO was effected with green light at 527 nm (PSS of *cis:trans* = 89:11 established by NMR analysis, for specifications see Figure 9), while irradiation with violet light at 400 nm (for specifications see Figure 7) can be applied to switch back to the *trans* state. Photoisomerization could also be performed selectively in aqueous LB broth (used herein as medium for bacterial growth), with no sign of fatigue evident over numerous cycles at 37 °C. With a photoswitchable aminopyrimidine in hand that can be photoisomerized in either direction with visible light, its antimicrobial activity was investigated. Interestingly, **12** showed increased activity against *E. coli* when compared to **2i** in both isomeric forms.

Furthermore, we noted a significant difference in anti-bacterial activity between the two forms remained at concentrations of 4–7 µM (Figure 3), with a genuine "activation" effect evident upon *trans-cis* isomerization with green light (translating into a change of MIC50 from 10 µM to 5 µM). While these results were obtained for pre-irradiation of the samples in the absence of bacteria, analogous experiments with true *in situ* irradiation after inoculation of bacteria yielded a similar effect (Figure 4), as photoisomerization with non-toxic green light could be achieved without influencing the bacterial growth with the applied light. This marks an important next step towards the reversible photocontrol of an antibacterial agent *in vivo* with biocompatible wavelengths of light.

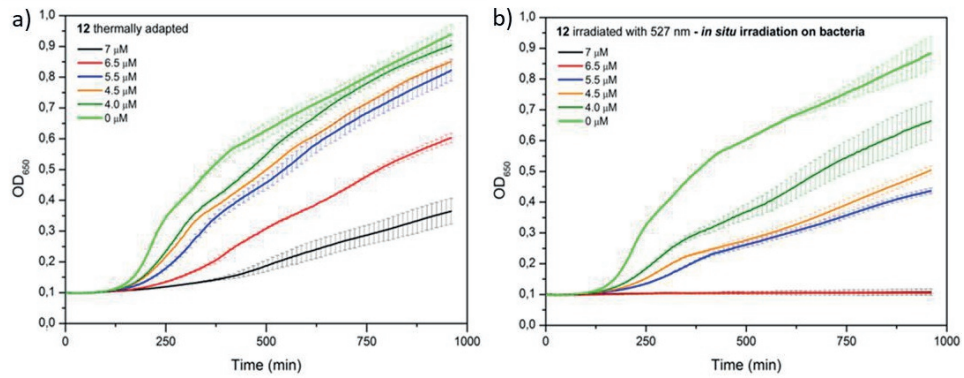

Figure 4. Bacterial growth curves of *E. coli* CS1562 at increasing concentrations of **12**. a) Samples after thermal adaptation. b) Samples after *in situ* irradiation with green light at λ = 527 nm in the presence of bacteria. Error bars show s.d. calculated from measurements in triplicate.

Having successfully realized control over bacterial growth with green light using photoresponsive aminopyrimidine **12**, we sought to take our approach a step further by red-shifting the wavelength of activation even more. For this purpose, diaminopyrimidine **13** (as a structural analogue of **2i** and **12**) was synthesized, featuring four chloro substituents in *ortho* positions of the azobenzene (see Scheme 2). Tetra-*ortho*-chloroazobenzenes have been reported to engage in *trans-cis* isomerization upon irradiation with red light between 630 and 660 nm.[74,76] Indeed, irradiation of 13 with red light at 652 nm effected photoisomerization to a PSS of *cis:trans* = 87:13 (in DMSO, Figures 5A and 5B), albeit after prolonged irradiation times of 2–3 h. Faster isomerization was observed for irradiation with green light at 527 nm; however, this only resulted in a PSS *cis:trans* ratio of about 1:1. A compromise between irradiation time and PSS for the *cis-trans* isomerization of **13** could be reached by using a strong white light source in combination with a filter cutting off wavelengths below 530 nm: Using this light source, a PSS of *cis:trans* = 69:31 could be reached within 10 min. Photoisomerization of **13** also proceeded cleanly in aqueous medium and without fatigue over numerous cycles.

Due to our interest in the farthest possible shift of our photoswitchable agents' response towards the red, we immediately focused on the influence of red light irradiation on the antibacterial activity of **13**. In that regard, initial experiments performed analogously to the other compounds in this study (two-fold dilution series in 96-wells plates) yielded disappointing results, with a noticeable but unsatisfactory difference in growth evident. However, we imagined that this lack of difference in activity before and after irradiation might well be due to ineffective photoswitching in the 96-wells plates, as the light source was usually positioned at a distance of 11.5 cm from the plate to ensure maximum coverage. To verify this assumption, one half of a divided stock solution of **13** in DMSO was irradiated for 2.5

h with red light at 652 nm at a distance < 1 cm, before treating bacteria with the two separate samples in two-fold dilution series.

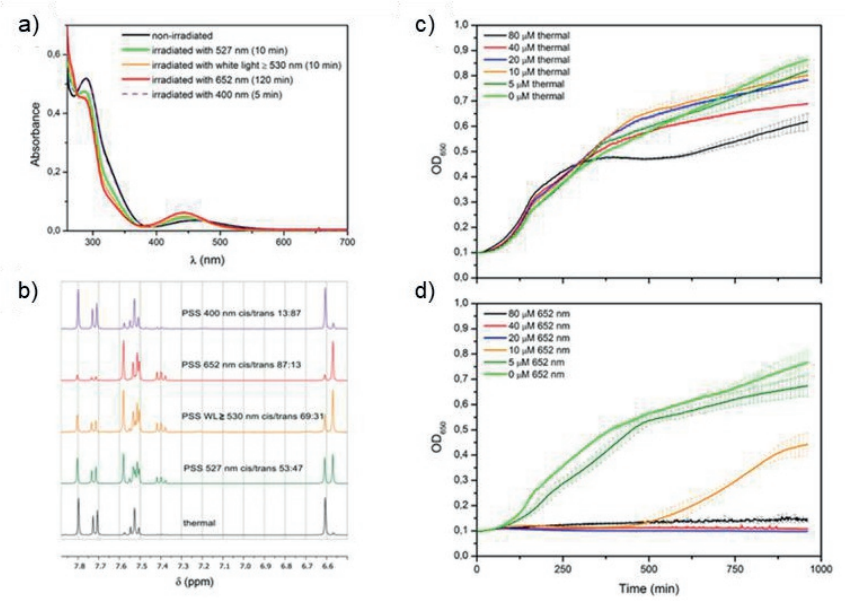

Figure 5. a) UV-Vis absorption spectra of **13** before and after irradiation with various light sources in DMSO. b) Partial ^{1}H NMR spectra of **13** before and after irradiation with various light sources in DMSO-d_6 c) Bacterial growth curves of *E. coli* CS1562 at increasing concentrations of **13** after thermal adaptation. d) Bacterial growth curves of *E. coli* CS1562 at increasing concentrations of **13** after irradiation with red light. Irradiation was performed on a solution of **13** in DMSO for 2.5 h with red light at λ = 652 nm. Error bars show s.d. calculated from measurements in triplicate.

To our delight, this experiment revealed a dramatic photoactivation effect: Whereas non-irradiated **13** remained largely inactive with a MIC50 > 80 µM (Figure 5C), red light-irradiated **13** induced bacteriostasis down to 20 µM, with an observed MIC50 of 10 µM (Figure 5D).

To exclude the possibility that factors such as changes in solubility upon photoisomerization have an undesired influence on the antibacterial activity of **13** in our experiments, we considered it vital to demonstrate that the photocontrol of its activity is reversible. Taking advantage of the fact that switching **13** back from its active *cis* form to the inactive *trans* form can be performed within the visible light range, experiments were conducted with violet light at 400 nm (cf. Figures 5A and 5B). This allowed us to treat bacteria with a red-light-irradiated, "activated" sample of **13** in two two-fold dilution series, before irradiating half of the inoculated bacteria with 400 nm light, evidently without harming the bacteria in the process (Figure 6B). We were pleased to find that, indeed, samples irradiated with violet light were

effectively "deactivated" again, with a MIC50 > 80 μM, just as previously observed for the *trans* isomer, properly restored (compared once again to the MIC50 = 10 μM of the active *cis* isomer protected from violet light irradiation, Figure 6A).

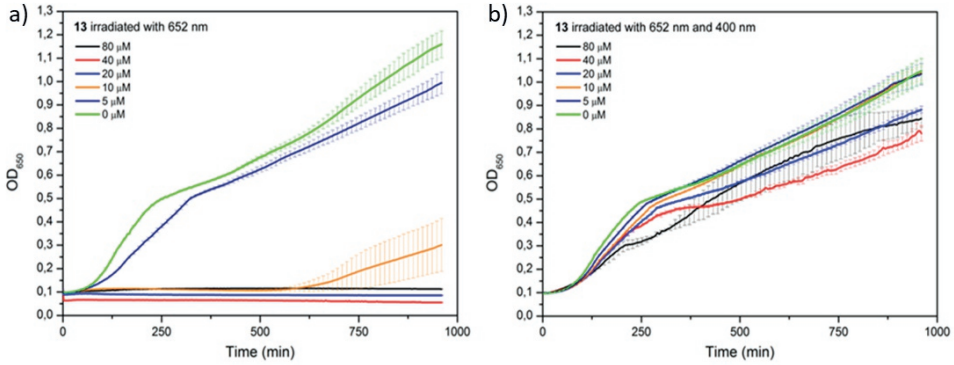

Figure 6. Two series of bacterial growth curves of *E. coli* CS1562 at increasing concentrations of **13** irradiated with red light at λ = 652 nm for 3 h in DMSO before treatment of bacteria. One series of bacteria a) was protected from further irradiation. The other series b) was irradiated with violet light at λ = 400 nm after inoculation. Error bars show s.d. calculated from measurements in triplicate.

While the inefficient photoisomerization of **13** with red light prevented us from conducting red light irradiation experiments in the presence of bacteria in our model *in vitro* system, the results presented herein mark a significant development in our ongoing efforts to create photoresponsive antibiotics, as we were able, for the first time, to control the activity (eight-fold difference) of an antibacterial agent with light beyond the 650 nm mark, which constitutes the lower margin of therapeutic window,[45,46] bringing us an important step closer to future *in vivo* control of photoswitchable antibiotics.

5.3 Conclusions

We successfully developed photoresponsive, antibacterial diaminopyrimidines bearing azobenzene photoswitches, whose activity can be controlled by light of various wavelengths. Identification of a UV light-responsive core structure with suitable antibacterial properties and subsequent, targeted modification of the photoswitch moiety lead us to structures whose activity could be increased upon irradiation with green and red light. Remarkably, for the first time, these compounds allowed for the full *in situ* photocontrol of antibacterial activity with green and violet light, making it possible to trigger both the "activation" as well as "deactivation" of the antibacterial agent in the presence of bacteria. Most significantly, diaminopyrimidine **13** revealed an at least eight-fold difference in activity before and after irradiation with red light (previous efforts in our group show that much lower differences are already sufficient for spatiotemporal patterning of bacteria).[33,34] More

importantly, apart from showcasing the effective "activation" of a biological agent otherwise inactive within the investigated concentration range, we were able to do so while also shifting the wavelength of activation from the UV range towards red light in the therapeutic window.

5.4 Experimental Section

5.4.1 General Remarks

For general remarks, see chapter 3.

5.4.2 Synthesis

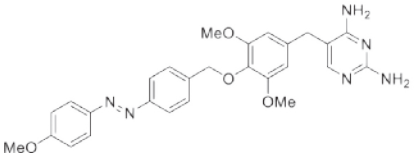

(E)-5-(3,5-dimethoxy-4-((4-((4-methoxyphenyl)diazenyl)benzyl)oxy)benzyl)pyrimidine-2,4-diamine (**2i**)

Following a modified procedure previously reported for the preparation of a different product,[67] KO*t*-Bu (44.6 mg, 0.398 mmol, 1.1 eq.) was added to a solution of 4-((2,4-diaminopyrimidin-5-yl)methyl)-2,6-dimethoxyphenol (100 mg, 0.362 mmol, 1 eq.) in 4 mL dry DMSO under nitrogen atmosphere and the resulting mixture stirred for 30 min at room temperature. Subsequently, (E)-1-(4-(bromomethyl) phenyl)-2-(4-methoxy-phenyl)-diazene (121 mg, 0.398 mmol, 1.1 eq.) was added to the reaction, and stirring at room temperature was continued for 4 h. The reaction mixture was then partitioned between water and EtOAc, the separated aqueous layer was extracted with EtOAc (3 × 20 mL), and the combined organic layers were washed with brine, dried over Na_2SO_4 and concentrated under reduced pressure. Purification by flash chromatography (DCM/MeOH 98:2 → 95:5) gave diaminopyrimidine **2i** as an orange solid (66.6 mg, 0.133 mmol, 37%).

Melting point: 209 – 211 °C.

^{1}H NMR (400 MHz, DMSO-d6): δ 7.90 (d, J = 8.9 Hz, 2H), 7.84 (d, J = 8.1 Hz, 2H), 7.64 (d, J = 8.1 Hz, 2H), 7.53 (s, 1H), 7.14 (d, J = 9.0 Hz, 2H), 6.59 (s, 2H), 6.15 (bs, 2H), 5.75 (bs, 2H), 4.94 (s, 2H), 3.87 (s, 3H), 3.75 (s, 6H), 3.55 (s, 2H).

^{13}C NMR (100 MHz, DMSO-d_6): δ 162.2, 162.0, 162.0, 155.2, 152.8, 151.4, 146.2, 140.9, 136.1, 134.5, 128.6, 124.5, 122.0, 114.6, 105.8, 105.8, 73.5, 55.9, 55.6, 33.0.

HRMS (ESI): m/z 501.2242 [501.2245 calcd. for $C_{27}H_{29}N_6O_4^+$ ($M+H^+$)].

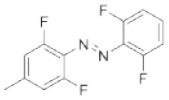

(E)-1-(2,6-difluoro-4-methylphenyl)-2-(2,6-difluorophenyl)diazene (**7**)

Following our previously reported procedure in a slightly modified way,[75] 3,5-difluorotoluene (512 mg, 4.00 mmol, 1 eq.) dissolved in 8 mL dry THF at -78 °C was slowly treated with a solution of *n*-BuLi (1.6 m in hexane, 2.5 mL, 4.00 mmol, 1 eq.), after which stirring was continued at -78 °C for 1 h. Solid 2,6-difluorobenzenediazonium tetrafluoroborate. (**5**, 912 mg, 4.00 mmol, 1 eq.) was then at once added to the reaction mixture, which was subsequently allowed to warm to room temperature over 1.5 h. The reaction was quenched with saturated aqueous $NaHCO_3$ solution, extracted with EtOAc (3 × 20 mL), and the combined organic layers were washed with brine, dried over Na_2SO_4 and concentrated under reduced pressure. After purification by flash chromatography (P/EtOAc 100:0 → 99:1 → 98:2), azobenzene **7** was obtained as a dark-red crystalline solid (766 mg, 2.86 mmol, 72%) consisting mainly of the *cis* isomer, which was used in the next step without thermal adaptation.

Melting point: 85 – 87 °C.

^{1}H NMR (400 MHz, DMSO-d$_6$): δ 7.65 – 7.54 (m, 1H), 7.35 (t, J = 9.6 Hz, 2H), 7.22 (d, J = 11.6 Hz, 2H), 2.41 (s, 3H).

^{13}C NMR (100 MHz, DMSO-d$_6$): δ 159.0 (dd, J = 7.7, 4.7 Hz), 156.4 (dd, J = 6.8, 4.6 Hz), 148.38 (t, J = 10.6 Hz), 135.8 (t, J = 10.6 Hz), 133.9 (t, J = 10.3 Hz), 131.5 (t, J = 9.7 Hz), 116.7 (dd, J = 20.0, 3.2 Hz), 116.3 (dd, J = 20.6, 2.9 Hz), 24.3.

^{19}F NMR (376 MHz, DMSO-d$_6$): δ -122.0 (d, J = 10.8 Hz), -122.3 (dd, J = 10.0, 6.1 Hz).

HRMS (ESI): m/z 269.0701 [269.0696 calcd. for $C_{13}H_9F_4N_2^+$ (M+H$^+$)].

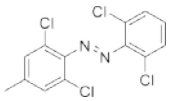

(E)-1-(2,6-dichloro-4-methylphenyl)-2-(2,6-dichlorophenyl)diazene (**8**)

In a procedure analogous to the preparation of **7**, reaction of 3,5-dichlorotoluene (593 mg, 3.68 mmol, 1 eq.) with *n*-BuLi and 2,6-dichlorobenzenediazonium tetrafluoroborate[75] (**6**, 961 mg, 3.68 mmol, 1 eq.) gave azobenzene **8** as a dark-red crystalline solid (916 mg, 2.74 mmol, 75%) consisting mainly of the *cis* isomer, which was used in the next step without thermal adaptation.

Melting point: 121 – 124 °C.

^{1}H NMR (400 MHz, DMSO-d$_6$): δ 7.69 (d, J = 8.1 Hz, 2H), 7.55 (s, 2H), 7.50 (t, J = 8.1 Hz, 1H), 2.39 (s, 3H).

^{13}C NMR (101 MHz, DMSO-d$_6$): δ 146.8, 143.9, 142.4, 130.9, 130.3, 129.8, 126.2, 125.8, 20.2.

HRMS (ESI): *m/z* 334.9490 [334.9485 calcd. for $C_{13}H_9Cl_4N_2^+$ (M+H$^+$)].

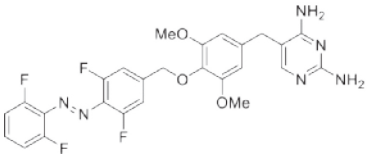

(E)-5-(4-((4-((2,6-difluorophenyl)diazenyl)-3,5-difluorobenzyl)oxy)-3,5-dimethoxybenzyl)pyrimidine-2,4-diamine (**12**)

Azobenzene **7** (268 mg, 1.00 mmol, 1 eq.), *N*-bromosuccinimide (178 mg, 1.00 mmol, 1 eq.) and AIBN (33.0 mg, 0.200 mmol, 20 mol%) were dissolved in 10 mL carbon tetrachloride under nitrogen atmosphere. The resulting mixture was heated to 85 °C with stirring for 60 h. After cooling to room temperature, the solvent was then removed under reduced pressure and the product purified by flash chromatography (P/EtOAc 98:2 → 96:4) to yield bromide **9** as a dark red solid (166 mg, 0.478 mmol, 48%). KO*t*-Bu (49.3 mg, 0.440 mmol, 1.1 eq.) was added to a solution of phenol **11** (111 mg, 0.400 mmol, 1 eq.) in 1.3 mL dry DMSO under nitrogen atmosphere and the resulting mixture was stirred for 30 min at room temperature. Subsequently bromide **9** (153 mg, 0.440 mmol, 1.1 eq.) was added to the reaction, and stirring at room temperature was continued for 4 h. The reaction mixture was then partitioned between water and EtOAc, the separated aqueous layer was extracted with EtOAc (3 × 30 mL), and the combined organic layers were washed with brine, dried over Na_2SO_4 and concentrated under reduced pressure. After purification by flash chromatography (DCM/MeOH 98:2 → 95:5), diaminopyrimidine **12** was obtained as a red-orange crystalline solid (207 mg, 0.382 mmol, 95%).

Melting point: 183 – 185 °C.

^{1}H NMR (400 MHz, DMSO-d$_6$): δ 7.63 (tt, *J* = 8.4, 6.1 Hz, 1H), 7.53 (s, 1H), 7.46 (d, *J* = 10.9 Hz, 2H), 7.37 (t, *J* = 9.3 Hz, 2H), 6.61 (s, 2H), 6.12 (bs, 2H), 5.71 (bs, 2H), 4.99 (s, 2H), 3.76 (s, 6H), 3.55 (s, 2H).

^{13}C NMR (100 MHz, DMSO-d$_6$): δ 162.2, 162.1, 155.9 (dd, *J* = 10.8, 4.3 Hz), 155.5, 153.3 (dd, *J* = 11.2, 4.4 Hz), 152.5, 145.1 (t, *J* = 9.9 Hz), 136.5, 134.3, 133.1 (t, *J* = 10.8 Hz), 130.7 (t, *J* = 10.0 Hz), 129.5 (t, *J* = 10.1 Hz), 113.2 (dd, *J* = 20.1, 3.4 Hz), 111.3 (dd, *J* = 21.1, 3.2 Hz), 105.7, 105.7, 72.5, 55.9, 33.0.

^{19}F NMR (376 MHz, DMSO-d$_6$): δ -121.4 (d, *J* = 10.8 Hz), -122.0 (dd, *J* = 10.0, 6.1 Hz).

HRMS (ESI): *m/z* 543.1762 [543.1762 calcd. for $C_{26}H_{23}F_4N_6O_3^+$ (M+H$^+$)].

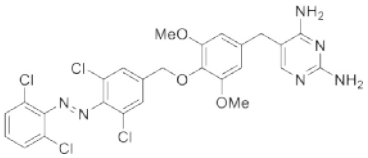

(E)-5-(4-((3,5-dichloro-4-((2,6-dichlorophenyl)diazenyl)benzyl)oxy)-3,5-dimethoxybenzyl)pyrimidine-2,4-diamine (**13**)

In a two-step procedure analogous to the preparation of **12**, reacting azobenzene **8** (305 mg, 0.913 mmol, 1 eq.) with *N*-bromosuccinimide (162 mg, 0.913 mmol, 1 eq.) and AIBN (16.0 mg, 45.7 µmol, 10 mol%) at 85 °C for 22 h first gave bromide **10** as a dark red solid (198 mg, 0.480 mmol, 53%). Bromide **10** (182 mg, 0.440 mmol, 1.1 eq.) was subsequently reacted with phenol **11** (111 mg, 0.400 mmol, 1 eq.) and KO*t*-Bu, after which purification by flash chromatography (DCM/MeOH 98:2 → 95:5) gave diaminopyrimidine **13** as an reddish brown solid (159 mg, 0.261 mmol, 65%).

Melting point: 215–217 °C.

^{1}H NMR (400 MHz, DMSO-d$_6$): δ 7.80 (s, 2H), 7.72 (d, J = 8.1 Hz, 2H), 7.56 – 7.49 (m, 2H), 6.61 (s, 2H), 6.13 (bs, 2H), 5.72 (bs, 2H), 4.99 (s, 2H), 3.76 (s, 6H), 3.54 (s, 2H).

^{13}C NMR (101 MHz, DMSO-d$_6$): δ 162.2, 162.2, 155.7, 152.5, 146.6, 145.3, 142.4, 136.5, 134.2, 131.2, 129.9, 128.4, 126.0, 125.9, 105.7, 105.7, 72.2, 55.9, 33.0.

HRMS (ESI): m/z 609.0552 [609.0551 calcd. for $C_{26}H_{23}Cl_4N_6O_3^+$ ($M+H^+$)].

5.4.3 Chemical actinometry and quantum yield determination

An aqueous 0.05 M H_2SO_4 solution containing 6 mM, 12 mM and 150 mM $K_3[Fe(C_2O_4)_3]$ (2 or 3 mL, 1 cm quartz cuvette), respectively for 365, 400 and 527 nm, was irradiated at 20 °C for a given period of time in the dark with the respective wavelength. A volume of 20, 10, 20 µL was taken respectively for 365, 400 and 527 nm and diluted to 2.0 mL with an aqueous 0.5 M H_2SO_4 solution containing phenanthroline (1 g/L) and NaOAc (122.5 g/L). The absorption at λ = 517 nm was measured and compared to an identically prepared non-irradiated sample. The concentration of $[Fe(phenanthroline)_3]^{2+}$ complex was calculated using its molar absorptivity (ε = 11100 m^{-1} cm^{-1}). This concentration corresponded to the concentration of Fe^{2+} ions that had formed upon irradiation divided by 100, 200, 100 respectively for 365, 400 and 527 nm. For 527 nm the probabililty factor at λ = 527 nm was taken into account[77] and the theoretical concentration of Fe^{2+} formed upon irradiation at all given time-points was calculated (probability factor = $1\text{-}10^{-Abs(527nm)}$). The Fe^{2+} ion concentration was plotted versus time and the following slope, obtained by linear fitting to the equation y = ax + b using Origin software (Figure 7-9), equals the rate of formation for the given wavelengths at standardized conditions. These rates can be converted in light doses by taking into account the

quantum yield and area of irradiation which is 2, 3 and 3 cm^2 respectively for 365, 400 and 530 nm. Subsequently, the energy per moles of photons at a given wavelength ($E_{mole\ of\ photons}$= N_A x h x ν = N_A x h x c / λ) is taken to convert this into J s^{-1} cm^{-2}.

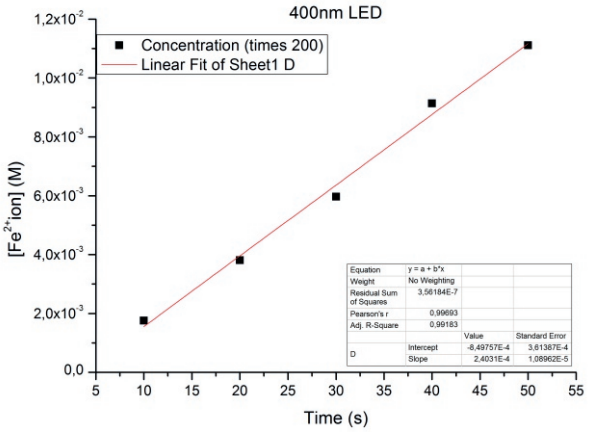

Figure 7. Concentration of Fe^{2+} ions measured after five different irradiation times (10, 20, 30, 40, 50 s) with 400 nm light. The slope of the plot corresponds to the rate of Fe^{2+} ion formation: 2.40 × 10^{-4} M s^{-1} ± 1.08 × 10^{-5} M s^{-1} = 7.20 x 10^{-7} mole s^{-1} ± 3.24 x 10-8 mole s^{-1}. Following ϕ(ferrioxalate at 400 nm) = 1.14 and the area of irradiation = 3 cm^2 and $E_{(mole\ of\ photons\ at\ 400\ nm)}$ = 2.99 x 10^5 this gives the light dose at 400 nm of 6.29 x 10^{-3} J s^{-1} cm^{-2}.

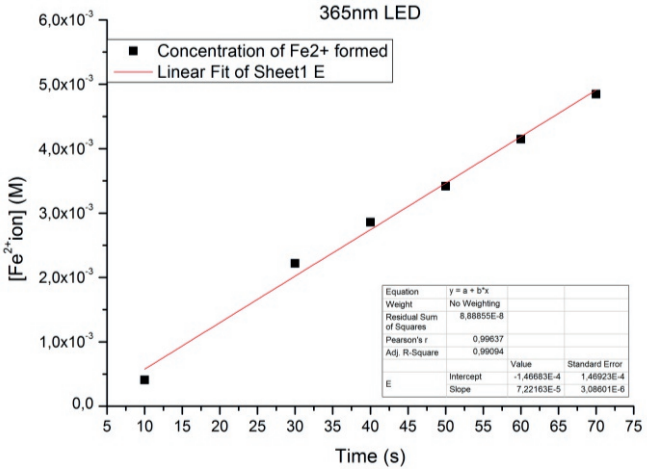

Figure 8. Concentration of Fe^{2+} ions measured after six different irradiation times (10, 30, 40, 50, 60, 70 s) with 365 nm light. The slope of the plot corresponds to the rate of Fe^{2+} ion formation: 7.22 × 10^{-5} M s^{-1} ± 3.08 × 10^{-6} M s^{-1} = 1.44 x 10^{-7} mole s^{-1} ± 6.16 x 10^{-9} mole

s^{-1}. Following ϕ(ferrioxalate at 365 nm)= 1.21 and the area of irradiation = 2 cm^2 and $E_{(mole\ of\ photons\ at\ 365\ nm)}$ = 3.28 x 10^5 this gives the light dose at 365 nm of 1.95 x 10^{-3} J s^{-1} cm^{-2}.

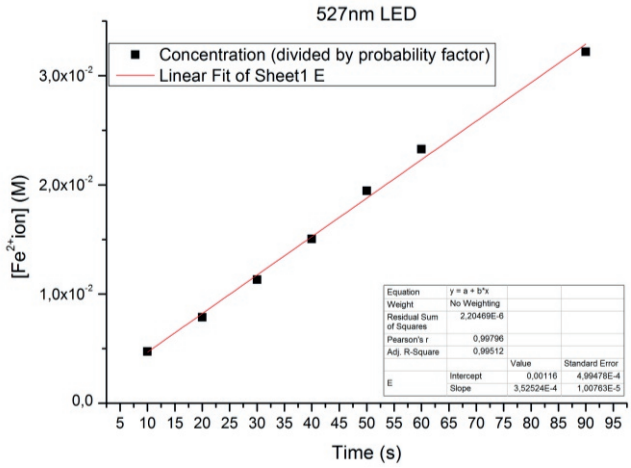

Figure 9. Concentration of Fe^{2+} ions measured after seven different irradiation times (10, 20, 30, 40, 50, 60, 90 s) with 527 nm light. The slope of the plot corresponds to the rate of Fe^{2+} ion formation: 3.52 × 10^{-4} M s^{-1} ± 1.00 × 10^{-5} M s^{-1} = 1.05 x 10^{-6} mole s^{-1} ± 3 x 10^{-8} mole s^{-1}. Following ϕ(ferrioxalate at 527 nm)= 0.53 and the area of irradiation = 3 cm^2 and $E_{(mole\ of\ photons\ at\ 527\ nm)}$ = 2.27 x 10^5 this gives the light dose at 527 nm of 1.49 x 10^{-1} J s^{-1} cm^{-2}.

A solution of (*trans*)-**2i** was irradiated with the Thorlab model F365F1 high-power LED under identical standardized conditions as with the actinometry at concentrations high enough to absorb all incident light (absorbance at 365 ≥ 2). The absorbance decrease at λ = 385 nm was monitored over time by UV-Vis spectroscopy. The molar absorptivities at λ = 365 nm [(*trans*)-**2i**, ε_{trans} = 18111 m^{-1} cm^{-1}; for (*cis*)-**2i**, ε_{cis} = 1282 m^{-1} cm^{-1}] were used to calculate the concentration increase of (*cis*)-**2i** according to Δc = Δabs/(ε_{trans} + ε_{cis}). The initial concentration increase was plotted versus time (Figure 10) and the slope, the rate of formation of *cis* isomer over time, was obtained by linear fitting to the equation y = ax + b using Origin software. The photochemical quantum yield for **2i** ($\varepsilon_{trans\text{-}cis}$) was calculated by comparison of the rate of formation of (*cis*)-**2i** with the rate of Fe^{2+} ion formation at identical conditions upon 365 nm irradiation from potassium ferrioxalate using the known quantum yield for the ferrioxalate at the given wavelength (ϕ = 1.21).[78,79] Calculation of the quantum yield for the reverse reaction at 365 nm can be performed following $\varepsilon_{cis\text{-}trans}$ = $\varepsilon_{trans\text{-}cis}$ * ε_{trans}*[2i$_{trans}$]/(ε_{cis}*[2i$_{cis}$]) where the concentrations of **2i** are taken at given PSS (1:99, *trans:cis*).

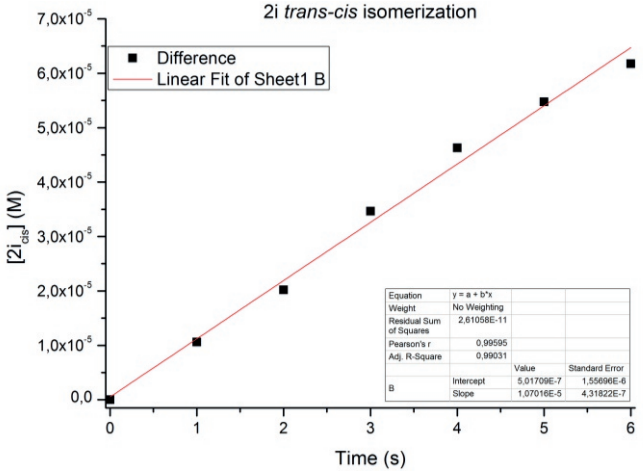

Figure 10. Plot of the concentration of (*cis*)-**2i** as a function of time during λ_{max} = 365 nm irradiation of a solution of (*trans*)-**2i** in DMSO (c = 1.33 × 10^{-4} m, 1 cm quartz cuvette) obtained by monitoring the absorption decrease at λ = 385 nm. The slope of the plot corresponds to the *trans-cis* isomerisation rate: 1.07 × 10^{-5} M s^{-1} ± 4.31 × 10^{-7} M s^{-1} = 3.21 x 10^{-8} mole s^{-1} ± 1.29 x 10^{-9} mole s^{-1}. Correlation of this rate to the rate of ferrioxalate consumption at these standardized conditions with 365 nm and the ferrioxalate quantum yield at the given wavelength gives a quantum yield of 18% for *trans-cis* isomerization and logically a quantum yield of 2.5% for *cis-trans* isomerization.

5.5 References

(1) Alanis, A. J. *Arch. Med. Res.* **2005**, *36*, 697–705.

(2) Carlet, J.; Collignon, P.; Goldmann, D.; Goossens, H.; Gyssens, I. C.; Harbarth, S.; Jarlier, V.; Levy, S. B.; N'Doye, B.; Pittet, D.; Richtmann, R.; Seto, W. H.; van der Meer, J. W. M.; Voss, A. *Lancet* **2011**, *378*, 369–371.

(3) Smith, R.; Coast, J. *BMJ* **2013**, *346*, f1493.

(4) Cantas, L.; Shah, S. Q. A.; Cavaco, L. M.; Manaia, C. M.; Walsh, F.; Popowska, M.; Garelick, H.; Bürgmann, H.; Sørum, H. *Front. Microbiol.* **2013**, *4*, 96.

(5) Kummerer, K. *J. Antimicrob. Chemother.* **2003**, *52*, 5–7.

(6) Dancer, S. J. *Lancet Infect. Dis.* **2004**, *4*, 611–619.

(7) Kemper, N. *Ecol. Indic.* **2008**, *8*, 1–13.

(8) Norrby, S. R.. *Eur. J. Clin. Microbiol. Infect. Dis.* **1991**, *10*, 378–383.

(9) Mehlhorn, A. J.; Brown, D. A. *Ann. Pharmacother.* **2007**, *41*, 1859–1866.

(10) Press Announcements - FDA updates warnings for fluoroquinolone antibiotics https://www.fda.gov/NewsEvents/Newsroom/PressAnnouncements/ucm513183.htm (accessed Apr 9, 2018).

(11) Paiva, J. A.; Pereira, J. M. *Crit. Care Med.* **2015**, *43*, 708–710.

(12) Khaliq, Y.; Zhanel, G. G. *Clin. Infect. Dis.* **2003**, *36*, 1404–1410.

(13) Ali, A. K. *Ann. Epidemiol.* **2014**, *24*, 279–285.

(14) Lewis, K. *Nat. Rev. Drug Discov.* **2013**, *12*, 371–387.

(15) Walsh, C. T.; Wencewicz, T. A. *J. Antibiot. (Tokyo).* **2014**, *67*, 7–22.

(16) Velema, W. A.; Szymanski, W.; Feringa, B. L. *J. Am. Chem. Soc.* **2014**, *136*, 2178–2191.

(17) Broichhagen, J.; Frank, J. A.; Trauner, D. *Acc. Chem. Res.* **2015**, *48*, 1947–1960.

(18) Lerch, M. M.; Hansen, M. J.; van Dam, G. M.; Szymanski, W.; Feringa, B. L. *Angew. Chem., Int. Ed.* **2016**, 55, 10978–10999.

(19) Contreras-García, E.; Martínez-López, D.; Alonso, C. A.; Lozano, C.; Torres, C.; Rodríguez, M. A.; Campos, P. J.; Sampedro, D. *European J. Org. Chem.* **2017**, *2017*, 4719–4725.

(20) Zhao, Y.; Farrer, N. J.; Li, H.; Butler, J. S.; McQuitty, R. J.; Habtemariam, A.; Wang, F.; Sadler, P. J. *Angew. Chem., Int. Ed.* **2013**, 52, 13633–13637.

(21) Haimei Chen; John A. Parkinson; Simon Parsons; Robert A. Coxall; Robert O. Gould, A.; Sadler, P. J. *J. Am. Chem. Soc.* **2002**, *124*, 3064–3082.

(22) Dickerson, M.; Sun, Y.; Howerton, B.; Glazer, E. C. *Inorg. Chem.* **2014**, *53*, 10370–10377.

(23) Wachter, E.; Heidary, D. K.; Howerton, B. S.; Parkin, S.; Glazer, E. C. *Chem. Commun.* **2012**, *48*, 9649.

(24) Knoll, J. D.; Turro, C. *Coord. Chem. Rev.* **2015**, *282–283*, 110–126.

(25) Knoll, J. D.; Albani, B. A.; Turro, C. *Acc. Chem. Res.* **2015**, *48*, 2280–2287.

(26) Karaoun, N.; Renfrew, A. K. *Chem. Commun.* **2015**, *51*, 14038–14041.

(27) Tinajero-Trejo, M.; Rana, N.; Nagel, C.; Jesse, H. E.; Smith, T. W.; Wareham, L. K.; Hippler, M.; Schatzschneider, U.; Poole, R. K. *Antioxid. Redox Signal.* **2016**, *24*, 765–780.

(28) Halpenny, G. M.; Heilman, B.; Mascharak, P. K. *Chem. Biodivers.* **2012**, *9*, 1829–1839.

(29) Meisel, P.; Kocher, T. *J. Photochem. Photobiol. B.* **2005**, *79*, 159–170.

(30) Harris, F.; Pierpoint, L. *Med. Res. Rev.* **2012**, *32*, 1292–1327.

(31) Wainwright, M. *Int. J. Antimicrob. Agents* **2010**, *36*, 14–18.

(32) Nagata Md, J. Y.; Hioka, N.; Kimura, E.; Batistela, R.; Sano, R.; Terada, S.; Graciano, A. X.; Baesso, M. L.; Hayacibara, M. F. *Photodiagnosis Photodyn. Ther.* **2011**, *9*, 122–131.

(33) Velema, W. A.; van der Berg, J. P.; Hansen, M. J.; Szymanski, W.; Driessen, A. J. M.; Feringa, B. L. *Nat. Chem.* **2013**, 5, 924–928.

(34) Velema, W. A.; Hansen, M. J.; Lerch, M. M.; Driessen, A. J. M.; Szymanski, W.; Feringa, B. L. *Bioconjug. Chem.* **2015**, *26*, 2592–2597.

(35) Babii, O.; Afonin, S.; Berditsch, M.; Reiβer, S.; Mykhailiuk, P. K.; Kubyshkin, V. S.; Steinbrecher, T.; Ulrich, A. S.; Komarov, I. V. *Angew. Chem., Int. Ed.* **2014**, *53*, 3392–3395.

(36) Weston, C. E.; Krämer, A.; Colin, F.; Yildiz, Ö.; Baud, M. G. J.; Meyer-Almes, F.-J.; Fuchter, M. J. *ACS Infect. Dis.* **2017**, *3*, 152–161.

(37) Hansen, M. J.; Velema, W. A.; de Bruin, G.; Overkleeft, H. S.; Szymanski, W.; Feringa, B. L. *ChemBioChem* **2014**, *15*, 2053–2057.

(38) Szymanski, W.; Ourailidou, M. E.; Velema, W. A.; Dekker, F. J.; Feringa, B. L. *Chem. A Eur. J.* **2015**, *21*, 16517–16524.

(39) Borowiak, M.; Nahaboo, W.; Reynders, M.; Nekolla, K.; Jalinot, P.; Hasserodt, J.; Rehberg, M.; Delattre, M.; Zahler, S.; Vollmar, A.; Trauner D., Thorn-Seshold O. *Cell* **2015**, *162*, 403–411.

(40) Reiner, A.; Isacoff, E. Y. *Nat. Chem. Biol.* **2014**, *10*, 273–280.

(41) Carroll, E. C.; Berlin, S.; Levitz, J.; Kienzler, M. A.; Yuan, Z.; Madsen, D.; Larsen, D. S.; Isacoff, E. Y. *Proc. Natl. Acad. Sci.* **2015**, *112*, 776–785.

(42) Polosukhina, A.; Litt, J.; Tochitsky, I.; Nemargut, J.; Sychev, Y.; De Kouchkovsky, I.; Huang, T.; Borges, K.; Trauner, D.; Van Gelder, R. N.; Kramer, R. H. *Neuron* **2012**, *75*, 271–282.

(43) Tochitsky, I.; Polosukhina, A.; Degtyar, V. E.; Gallerani, N.; Smith, C. M.; Friedman, A.; Van Gelder, R. N.; Trauner, D.; Kaufer, D.; Kramer, R. H. *Neuron* **2014**, *81*, 800–813.

(44) Matsumura, Y.; Ananthaswamy, H. N. *Toxicol. Appl. Pharmacol.* **2004**, *195*, 298–308.

(45) Kalka, K.; Merk, H.; Mukhtar, H. *J. Am. Acad. Dermatol.* **2000**, *42*, 389–413.

(46) Weissleder, R. *Nat. Biotechnol.* **2001**, *19*, 316–317.

(47) Hitchings, G. H.; Smith, S. L. *Adv. Enzyme Regul.* **1980**, *18*, 349–371.

(48) Kompis, I. M.,; Islam, K.; Then, R. L. *Chem. Rev.*, **2005**, *105*, 593–620

(49) Amyes, S. G.; Smith, J. T. *Antimicrob. Agents Chemother.* **1974**, *5*, 169–178.

(50) Kwon, Y. K.; Lu, W.; Melamud, E.; Khanam, N.; Bognar, A.; Rabinowitz, J. D. *Nat. Chem. Biol.* **2008**, *4*, 602–608.

(51) Kwon, Y. K.; Higgins, M. B.; Rabinowitz, J. D. *ACS Chem. Biol.* **2010**, *5*, 787–795.

(52) Zhou, W.; Scocchera, E. W.; Wright, D. L.; Anderson, A. C. *MedChemComm* **2013**, *4*, 908.

(53) Yuthavong, Y. *Microbes Infect.* **2002**, *4*, 175–182.

(54) Bolstad, D. B.; Bolstad, E. S.; Wright, D. L.; Anderson, A. C. *Expert Opin. Ther. Pat.* **2008**, *18*, 143–157.

(55) Walling, J. *Invest. New Drugs* **2006**, *24*, 37–77.

(56) Hagner, N.; Joerger, M. *Cancer Manag. Res.* **2010**, *2*, 293–301.

(57) Gonen, N.; Assaraf, Y. G. *Drug Resist. Updat.* **2012**, *15*, 183–210.

(58) Hitchings, G. H.; Elion, G. B.; Vanderwerff H.; Falco, E. A. *J. Biol. Chem.* **1948**, *174*, 765–766.

(59) Hitchings, G. H.; Elion, G. B.; Falco, E. A.; Russell, P. B.; Sherwood, M. B.; Vanderwerff, H. *J. Biol. Chem.* **1950**, *183*, 1–9.

(60) Roth, B.; Falco, E. A.; Hitchings, G. H.; Bushby, S. R. M. *J. Med. Pharm. Chem.* **1962**, *5*, 1103–1123.

(61) Bushby, S. R.; Hitchings, G. H *Br. J. Pharmacol. Chemother.* **1968**, *33*, 72–90.

(62) Burchall, J. J.; Hitchings, G. H. *Mol. Pharmacol.* **1965**, *1* ,126-136.

(63) Gleckman, R.; Blagg, N.; Joubert, D. W. *Pharmacother. J. Hum. Pharmacol. Drug Ther.* **1981**, *1*, 14–19.

(64) Huovinen, P. *Antimicrob. Agents Chemother.* **1987**, *31*, 1451–1456.

(65) Sundqvist, M.; Geli, P.; Andersson, D. I.; Sjolund-Karlsson, M.; Runehagen, A.; Cars, H.; Abelson-Storby, K.; Cars, O.; Kahlmeter, G. *J. Antimicrob. Chemother.* **2010**, *65*, 350–360.

(66) Miller, L. W.; Cai, Y.; Sheetz, M. P.; Cornish, V. W. *Nat. Methods* **2005**, *2*, 255–257.

(67) Liu, W.; Li, F.; Chen, X.; Hou, J.; Yi, L.; Wu, Y.-W. A *J. Am. Chem. Soc.* **2014**, *136*, 4468–4471.

(68) Siewertsen, R.; Neumann, H.; Buchheim-Stehn, B.; Herges, R.; Näther, C.; Renth, F.; Temps, F. *J. Am. Chem. Soc.* **2009**, *131*, 15594–15595.

(69) Yang, Y.; Hughes, R. P.; Aprahamian, I. *J. Am. Chem. Soc.* **2014**, *136*, 13190–13193.

(70) Beharry, A. A.; Woolley, G. A*Chem. Soc. Rev.* **2011**, *40*, 4422–4437.

(71) Dong, M.; Babalhavaeji, A.; Samanta, S.; Beharry, A. A.; Woolley, G. A. *Acc. Chem. Res.* **2015**, *48*, 2662–2670.

(72) Bléger, D.; Hecht, S. *Angew. Chem., Int. Ed.* **2015**, *54*, 11338–11349.

(73) Bléger, D.; Schwarz, J.; Brouwer, A. M.; Hecht, S. *J. Am. Chem. Soc.* **2012**, *134*, 20597–20600.

(74) Samanta, S.; Beharry, A. A.; Sadovski, O.; McCormick, T. M.; Babalhavaeji, A.; Tropepe, V.; Woolley, G. A. *J. Am. Chem. Soc.* **2013**, *135*, 9777–9784.

(75) Hansen, M. J.; Lerch, M. M.; Szymanski, W.; Feringa, B. L. *Angew. Chem., Int. Ed.* **2016**, *55*, 13514–13518.

(76) Konrad, D. B.; Frank, J. A.; Trauner, D. *Chem. - A Eur. J.* **2016**, *22*, 4364–4368.

(77) Hopkins, S. L.; Siewert, B.; Askes, S. H. C.; Veldhuizen, P.; Zwier, R.; Heger, M.; Bonnet, S. *Photochem. Photobiol. Sci.* **2016**, *15*, 644–653.

(78) Hatchard, C. G.; Parker, C. A. *Proc. R. Soc. A Math. Phys. Eng. Sci.* **1956**, *235*, 518–536.

(79) Montalti, M.; Credi, A.; Prodi, L.; Gandolfi, M. T.; Michl, J.; Balzani, V. *Handbook of Photochemistry*, **2006**.